PROCEEDINGS OF SCIENCE

RXTE observations of Cyg X-3

S. Özdemir*
Ahi Evran University, Faculty of Arts and Sciences, Department of Physics, Kırşehir, Turkey
E-mail: sozdemir@ahievran.edu.tr

M. Méndez
Kapteyn Astronomical Institute, University of Groningen, PB 800, 9700 AV Groningen, the Netherlands

M. van der Klis
Astronomical Institute "Anton Pannekoek", University of Amsterdam, Postbus 94249, 1090 GE Amsterdam, the Netherlands

N.E. White
NASA Goddard Space Flight Center, MD, USA

Timing data analysis of the bright X-ray source Cyg X-3 based on RXTE/PCA was presented. The observations were carried out in August 1996 and February 1997. All observations showed the $4.^{h}8$ modulation due to the orbital period of the system with count rate ranging from ~ 900 to ~ 6000 cnt s^{-1}. Almost all power spectra, the most sensitive timing results of Cyg X-3, may be well explained by pure Poisson noise above ~ 0.2 Hz and a power-law below ~ 0.2 Hz. During the February 1997, when the source was brightest in one part of the observations, it showed a temporary flickering-like behaviour with a period of ~ 70 s. A detailed study of the timing properties of Cyg X-3 as a function of count rate, orbital phase and photon energy was presented. The flickering-like behaviour seemed to be a dominant effect in describing the level and shape of the power spectra below ($<\sim 0.2$ Hz).

The Extreme sky: Sampling the Universe above 10 keV - extremesky2009,
October 13-17, 2009
Otranto (Lecce) Italy

*This work was performed during one of the authors' (SÖ) visit to the Astronomical Institute "Anton Pannekoek", University of Amsterdam as a guest investigator under a BDP grant by The Scientific and Technical Research Council of Turkey (TÜBITAK)

PoS(extremesky2009)068

1. Introduction

Cyg X-3 (=V1521 Cyg) was first discovered as an X-ray source by Giacconi et al. ([1967]), and as a radio source by Gregory et al. ([1972]). Although Cyg X-3 is at a distance greater than 8 kpc (Bonnet-Bidaud & Chardin [1988]) and located in the galactic plane, it is bright enough to be observed in all wavelengths except in the optical region. In the direction of Cyg X-3 the A_v is $> 20^m$ (Becklin et al. [1973]; van Kerkwijk [1993]).

Cyg X-3 can be observed in radio as a strong source, where it sometimes displays jet–like outbursts emanating from a central object at $\sim 0.3c$ (Schalinski et al. [1995]). The most recent radio outbursts in Cyg X-3 occurred on February 4^{th} (Ghigo et al. [1997]), just 17 days before our February observations. The first millimetre observations with partially simultaneous radio flux measurements were presented by Fender et al. ([1995]).

In [1973], van den Heuvel & de Loore proposed a model for Cyg X-3 where the system is composed of a compact object and a helium star of several solar masses in a late evolutionary stage of massive X-ray binaries. Using I and K band spectroscopy van Kerkwijk et al. ([1996]) confirmed that the optical component of the system is a Wolf-Rayet star, as identified spectral type of WN6/7 to WN4/5. They describe the IR emission of the system using a model, in which the companion of the X-ray source is a WR star whose wind is ionized by the X-ray source, except for the part in the star's shadow.

Cyg X-3 has a 4.8 hour orbital period observable in X-rays and IR (Becklin et al. [1973]). The X-ray modulation and its changes with time were investigated by numerous authors; see van der Klis & Bonnet-Bidaud ([1981]), Bonnet-Bidaud & van der Klis ([1981]), van der Klis & Bonnet-Bidaud ([1982]); see also Bonnet-Bidaud & Chardin ([1988]), and van der Klis ([1993]) for reviews.

Smit & van der Klis ([1996]) studied the X-ray colour-colour diagram of Cyg X-3. They found that the X-ray spectral variations in Cyg X-3 also have a 4.8 hour period and lead to the source performing a loop in the colour-colour diagram every 4.8 hours.

Presumably due to the scattering of the X-rays in the dense stellar wind within which Cyg X-3 embedded, it stands out among X-ray light curves by showing very little variability on time scales of seconds or less. van der Klis & Jansen ([1985]) discerned quasi-periodic oscillations with periods in the $50-1500$ s range superimposed on the X-ray light curve of Cyg X-3 using EXOSAT, but on shorter time scales than this, variability, if any is extremely weak.

Neither Kitamoto et al. ([1992]) nor Berger & van der Klis ([1994]) could found any short term variability in the timing data of Cyg X-3 carried out by GINGA and EXOSAT, respectively. For this reason, Cyg X-3 has defied classifications up to now; in the absence of X-ray pulsations or bursts, quasi–periodic oscillations or even broad noise support it has not even been possible to decide whether the source is a neutron star or a black hole.

In a recent study of timing analysis carried out by Stark & Saia ([2002]), no periodic or quasi-periodic oscillations were found on the basis of RXTE data. They propose to use the high frequency timing noise to put a constraint on the size of the X-ray emitting region and on the scattering atmosphere of the optical companion.

Vilhu et al. ([2003]) presented first INTEGRAL results of Cyg X-3 supported by simultaneous RXTE data. They fit their broad-band X-ray and $\gamma-$ray spectra with physical models of thermal

Comptonization and Compton reflection, which indicate black hole binaries at high Eddington rates. Cyg X-3 was also studied to solve the problem of strong and complex neutral and ionized absorption in the direction of the system (Szostek, Zdziarski & Lachowicz, [2004]). They used RXTE's public data of Cyg X-3 and divided them into four groups according to the shape of the PCA/HEXTE spectrum.

In the present work, we analyse high time resolution observations of Cyg X-3 with the Rossi X-ray Timing Explorer (RXTE). The observations have the most sensitive rapid time variability study of Cyg X-3. The power spectrum was studied as a function of count rate, orbital phase and photon energy. No variability is detected in the power spectra up to the Nyquist frequency (32 768 Hz) except for a power law below ~ 0.2 Hz and for one oscillation seen in one part of February observations. We use this information to set constrains on the properties of the scattering material around the source. Cyg X-3, as the only 'quite' bright celestial X-ray source, is excellent for calibration of instrumental fast-timing properties.

2. Observations

The observations were carried out using the Proportional Counter Array (PCA) on board of NASA's RXTE. The PCA consists of 5 Proportional Counter Units (PCUs), each of which has an effective area of approximately 1400 cm^2 and a 1° FWHM field of view. The observations were made on 24–30 August 1996 and 21–22 February 1997, during which RXTE made 6 and 2 observations of Cyg X-3, respectively, with a total exposure time of ~ 210000 s. In all cases the observations covered the $\sim 2-97$ keV energy range. Table 1 gives the log of the observations. Observations 1 to 6 were obtained using Event (E) mode, where each photon was registered with a time resolution of $62\,\mu$s in 32 energy channels covering the full PCA energy range. For observations 7 and 8 the $2-13$ keV photons were registered in 3 separate channels with a time resolution of $250\,\mu$s (Single Bit mode, SB), while the high energy photons (above 13 keV) were recorded using E mode in 64 energy channels with $16\,\mu$s time resolution.

Observations 1–3, 7 and 8 covered the entire 4.8 hour orbital cycle except for the Earth occultation intervals, meanwhile observations 4–6 were shorter.

3. Analysis

In each observation, data segments with reduced count rates due to atmospheric occultation effects were removed before further analysis as we found that they might distort the shape of the power spectra. These data segments (10–20 s) were selected on the basis of their proximity to Earth occultations in the light curves. Data drop outs were removed on the basis of the data that correspond to zero count. To study the timing behaviour of Cyg X-3, we divided the remaining data into segments of 1048576 contiguous bins, preserving the full time resolution available in each case, and produced power spectra by Fourier-transforming each segment (see van der Klis [1988] for details) in a number of different energy bands (see below). From the resulting power spectra it seemed that the source only contributed to frequencies below ~ 0.2 Hz. In view of this result we analysed separately the power spectra below and above that frequency to check if there was any source contribution at higher frequencies.

Table 1: Log of the observations. Day Number 1=Jan 1st. In observation 7, segment 1, the source reached a maximum count rate around 6000 cnts

Nr. of Obs.	Start UT (yr/dy hr : min)	Stop UT (yr/dy hr : min)	Mean flux $(2-97\,\mathrm{keV})$ cnt rate $\pm$ std.dev.
1	96/237 10 : 37	96/237 16 : 34	2013 ± 505
2	96/239 03 : 15	96/239 15 : 27	2327 ± 539
3	96/240 05 : 56	96/240 18 : 17	2550 ± 659
4	96/241 15 : 36	96/241 19 : 57	2434 ± 713
5	96/242 15 : 49	96/242 19 : 16	2277 ± 686
6	96/243 15 : 41	96/243 19 : 43	2748 ± 796
7	97/52 02 : 02	97/52 09 : 25	$4997^{a} \pm 715$
8	97/52 18 : 21	97/53 03 : 02	$4776^{a} \pm 722$

[a] SB+E mode

3.1 The power spectra at high frequency: Pure Poisson noise

All power spectra of Cyg X-3 at higher frequencies (> 0.2 Hz) turned out to be well represented by pure Poisson noise, the average power in this frequency range being slightly below 2, as would be expected from pure Poisson noise modified by instrumental dead time (*i.e.*, no source variability at all; Leahy et al. [1983]; see also Zhang ([1995]) for a discussion of the RXTE dead time effects).

3.1.1 The count rate dependence

The variable count rate of Cyg X-3 during its 4.8 h orbital period in observations 1–6 (from ~ 200 to $\sim 800\,\mathrm{cnt\,s^{-1}}$ per PCU over the whole energy range) makes it possible to study the average power in the power spectra for different count rate intervals. We measured the average power in 4 broad frequency intervals (0.04–16, 16–128, 128–1024, 1024–8192 Hz), and for each interval we fitted a linear relation to the average power as a function of the count rate (Fig. 1). We find a linear decrease of power with count between $\sim 200-800\,\mathrm{cnt\,s^{-1}}$ per PCU, except for the first frequency interval in which the powers are most probably influenced by the source variations. The fit results to the last three frequency intervals are approximately the same. We derive a limit to the the source contribution in the first frequency interval ($0.04-16$ Hz) by subtracting the average power over the 16–8192 Hz range from the 0.04–16 Hz power spectrum. The remaining power corresponded to a source variability of $(0.68 \pm 0.05)\%$ rms. A fit to the entire frequency range gives $P = (2.000 \pm 0.001) - (3.2 \pm 0.2) \times 10^{-5} \times$ count rate/PCU (the < 16 Hz power is negligible in this fit). This result may be compared to the one obtained in the Sec. 3.1.3, which shows that this is entirely consistent with pure dead time-modified Poisson noise.

3.1.2 The phase dependence

In Fig. 2 we plot the phase dependence of the average Poisson spectrum in four frequency

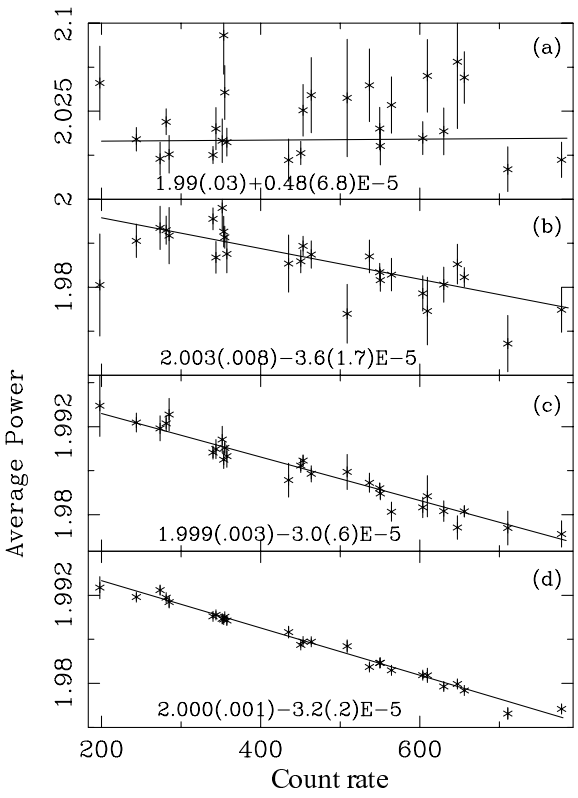

Figure 1: The count rate dependence of the average Poisson spectrum of observations 1–6 (2–97 keV). (**a**), (**b**), (**c**) and (**d**) refer to the frequency intervals of $0.04-16$, $16-128$, $128-1024$ and $1024-8192$ Hz, respectively. Only the first frequency interval might be affected by the source contamination. The equations of linear fits are shown at the bottom of each frame.

intervals. As the source count rate also depends on the orbital phase, we first have to subtract the count rate dependence to the average power for each phase interval, and then see if the residuals still show any dependence with the phase. The $y-$axis in this figure shows the difference between the observed power for each phase interval and the expected power for the corresponding count rate calculated using the linear fit given in Fig. 1. Except for the first frequency interval, the scattering of the individual points was consistent with zero within the error bars. In the first frequency interval the scattering was a bit larger than the error bars, may be due to variations in the power contributed by the source from one cycle to the other. We performed a linear fit to each frequency interval, and in all cases the slope was consistent with zero. This, together with the results of the previous subsections, indicates that the power spectra above $\sim$ 16 Hz are dominated by dead time effect, and that there is no contribution of the source to the power above this frequency.

3.1.3 Frequency dependence

Zhang ([1995]) showed that the power spectrum of a pure Poisson counting noise affected by simple paralyzable and non-paralyzable dead time can be expressed as:

$$P_j = P_1 - P_2\cos(2\pi j/N) + P_3\cos(4\pi j/N) + ... \tag{3.1}$$

where j is the frequency bin number in the power spectrum and N is the total number of bins. In the case of paralyzable dead time, every incident photon causes dead time and only P_1 and P_2 are different from zero, even if it is not detected by the detector. In the case of nonparalyzable dead time, only a detected event causes dead time, and all coefficients P_k are different from zero, but they rapidly go to zero as k increases.

In the case of the RXTE satellite, the Very Large Events (VLE), mainly due to particles detected by the PCUs, also contribute to the dead time. This effect can be modelled as an extra term in Eq. (3.1):

$$P_{\rm VLE} = 2\, r_{\rm VLE}\, r_0\, \tau_{\rm VLE}^2 \left[\frac{\sin \pi \tau_{\rm VLE} f}{\pi \tau_{\rm VLE} f}\right]^2 \tag{3.2}$$

where f is the frequency, $r_{\rm VLE}$ the VLE rate, r_0 the source count rate, and $\tau_{\rm VLE}$ the VLE window size. For a given observation $\tau_{\rm VLE}$ is fixed (it can take one of four values: 20, 55, 150, and 250 μs), and $r_{\rm VLE}$ and r_0 can be measured accurately. So, for a given observation, the VLE contribution to the power spectrum is known.

By combining equations Eq.(3.1) and Eq.(3.2) we can try to determine P_1, P_2, etc. from our data, and compare our results to those of Zhang ([1995]). In Fig. 3 fit results to the grand average power spectra are shown in whole 2–97 keV energy range. We divided our data in 7 slices according to the count rate (from 500 to 4000 cnt s^{-1} with 500 cnt s^{-1} intervals). For our observations the VLE window was fixed to 150 μs, and we determined for each power spectrum the value of $r_{\rm VLE} \times r_0$ and averaged them in each slice. Since these are well measured quantities, we first subtracted the VLE contribution to the power spectra according to Eq.(3.2), and then we fitted Eq.(3.1) for P_1 and P_2. We could not determine the VLE parameters or higher order terms in Eq.(3.1) than P_2 independently, due to the limited range of source count rate and the limited amount of data.

We find that P_1 is anticorrelated with the count rate, $P_1 = (2.000 \pm 0.001) - (3.35 \pm 0.25) \times 10^{-5} \times$ count rate/PCU. For P_2 we obtain 0.0009 ± 0.0001. The limited amount of data prevented us to get the dependence of P_2 with the count rate, however, it is clear that there is slight dependence of power on frequency.

Our results may be compared to those of Eq. (24) of Zhang et al. ([1995]). In the case of paralyzable dead time by using this equation we can derive a slope of 3.7×10^{-5} for P_1 vs. count rate (the bin size is 64 μs). Using this equation we can also calculate P_2 as 1.6×10^{-3} by entering an average count rate of 500 cnt rms^{-1}/PCU into the formula. This comparison shows that observational values are very close to theoretical one within the error bars.

3.1.4 Comparison to dead time model (P_1, P_2)

It seems clearly that the Poisson level is affected mainly by three parameters, *i.e.*, P_1, P_2, and $P_{\rm VLE}$. P_1 is the most efficient parameter among them and implicated into the formula as a constant whose value determined by dead time, count rate and binning time. Similarly, these variables define P_2. The effects of P_2 and $P_{\rm VLE}$ are more or less the same; however $P_{\rm VLE}$ has about 2 times of P_2 (see Table 2 to compare quantitatively these parameters). P_2 is small enough to be negligible since it does not influence very much in lower count rates (*i.e.*, $<$ 800 cnt s^{-1}/PCU) (see also Fig. 1 and Fig.2 of Zhang ([1995]) for graphical expressions of this).

When the 'rms' normalised spectra are performed, the calculated Poisson levels are used according to the affecting parameters and removed from the timing properties of Cyg X-3. A combination spectrum of observations 1–6 processed by this way seems to indicate that there is just Poisson noise > 16 Hz. Upper limits on source variability give (0.63 ± 0.40)%, (0.46 ± 0.12)%, and (0.28 ± 0.36)% rms in the frequency ranges 0.04–8192, 1–8192, 16–8192 Hz, respectively, with a 99% confidence level (3-σ).

3.2 The power spectra at low frequency: Power law VLFN

By using the results of the Sec. 3.1.3, we calculated and subtracted the Poisson level from each power spectrum. A combined power spectrum was obtained by adding the power spectra of observations 1 to 6. This rms normalized power spectrum fitted a power law VLFN (Very Low Frequency Noise) with an index of 1.74 ± 0.06 and fractional rms amplitude of (2.6 ± 0.3)% (between $0.001 - 1$ Hz) (see Fig. 3). The fit results to the power spectra for all individual observations are given in Table 2 together with the subtracted Poisson levels. Unlike the others, in observation 7, the VLFN deviates from the power law and produces a bumped noise (similar to Lorentzian distribution), which results from flickering in the first segment of the X-ray light curve. This part of the light curve is very similar to those already seen with EXOSAT by van der Klis & Jansen ([1985]) in which they detected transient QPOs with period of $50 - 1500$ s. The flickering is only seen when the source has the highest count rate in one part of observation 7. It makes the power spectrum ~ 10 times higher than the other rms normalized power spectra at frequencies $< \sim 0.2$ Hz (see Fig. 4). The count rate does not seem to have any influence on the level of the power spectra since segments 3, 4, and 5 of observation 7, and segments 1, 3, 4, and 6 of observation 8 do not show similar power as the first segment of observation 7 although they reach similar count rates, close to 6000 cnt s^{-1}.

3.2.1 The energy dependence

We analysed the energy dependence of the power spectra by dividing the observations four energy intervals and performing a similar analysis as in Sec. 3.2. No useful information could be derived from data above 29.5 keV. Therefore we excluded the data > 29.5 keV and sub-divided them into four energy intervals; 2–5.5, 5.5–11, 11–19, 19–29.5 keV. From this analysis we find that the VLFN slope is anticorrelated with the energy, while the VLFN rms amplitude increases with the energy (Fig. 5).

3.2.2 The count rate and phase dependence of the VLFN

The VLFN amplitude and slope was graphed versus count rate in various energy bands to see the count rate dependence of this component. We found no dependence on amplitude and slope of the count rate.

Similarly we analysed the phase dependence of the VLFN amplitude and slope. In this case, only the low energy interval ($2 - 13$ keV) was used (see Fig. 6). Segment 1 of observation 7, with an rms amplitude of (21.9 ± 3.6)%, deviates very much from the average. If this segment is excluded, neither the VLFN amplitude nor its slope has clear dependence on the orbital phase. However, the points between the 0.25–0.50 phase interval, which corresponds to flickering interval of Cyg X-3 (van der Klis & Jansen [1985]), show a small drop from the average.

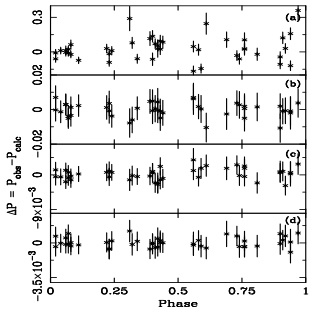

Figure 2: The phase dependence of the average Poisson spectrum. Frequency intervals are the same as in Fig. 1. Observations 7 and 8 are excluded. The folding was performed using the ephemeris given by Kitamoto et al. ([1995])

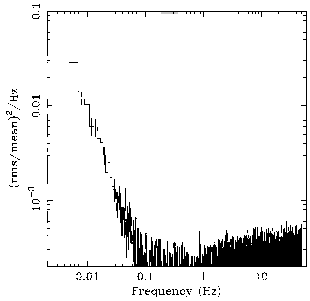

Figure 3: The grand average power spectrum of a combination of observations 1 to 6. The fit results in 16–8192 Hz range gives $P_1 = (1.98426 \pm .00011)$, $P_2 = (9.3 \pm 1.5)$E-4. $P_{\rm VLE}$, calculated from the appropriate count rate and VLE rate, is fixed as 2.05E-3. The nyquist frequency is 8192 Hz

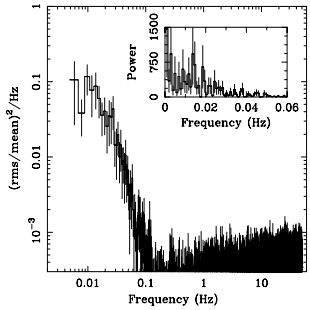

Figure 4: The power spectrum of segment 1 of obs7 seems to have a Lorentzian–like shape VLFN and a broad peak around 0.014 Hz (inset frame). The power spectrum which is combination of observations 1 to 6 gives a power law slope VLFN and no QPO (see Fig. 3). Energy interval of the figure is 2-13 keV. Note difference between Fig. 3 and 4 in $y-$scale

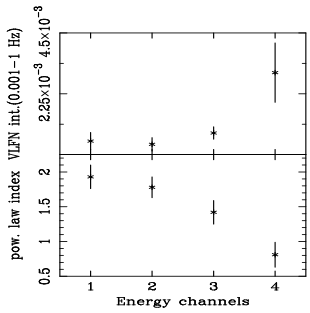

Figure 5: The variation of the VLFN integral (top panel) and index (bottom panel) with the photon energy. Each number in $x-$axis refers to the energy intervals of 2–5.5, 5.5–11, 11–19, 19–29.5 keV, respectively. Only observations 1 to 6 are included here.

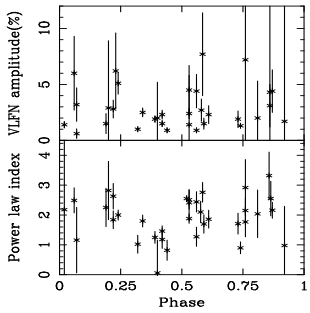

Figure 6: VLFN amplitude and power law index are shown as a function of phase of observations 1 to 8. Phase numbering is the same as in Fig. 2. Energies are $2-13$ keV for both panel. Average values of amplitude and power law index give (1.4 ± 0.6)% rms and 1.8 ± 0.5, respectively. VLFN amplitude of segment 1 (obs. 7) that has (21.9 ± 3.6)% rms is out of the graph

4. Results and discussion

We studied the power spectra of Cyg X-3 as a function of count rate, photon energy and orbital phase. Neither the high frequency part (dominated by Poisson counting noise) nor the low frequency part of the power spectra shows any clear dependence on the count rate and phase, but the VLFN component does change with photon energy. The average values of VLFN integral increase with energy whereas the power law index decreases up to >29.5 keV (see Fig. 5). The linear anticorrelation between the power level at high frequencies and the count rate is consistent with Poisson counting noise and dead time effects due to the instrument.

We did not detect the HFN component observed by Berger & van der Klis ([1994]) in any of our power spectra. They found an HFN with an amplitude of (3.3 ± 0.16)% rms between $1-256$ Hz. This confirms that HFN in the EXOSAT power spectra is instrumental as was already suggested by Berger & van der Klis ([1994]).

Segment 1 of observation 7 shows a specific behaviour compared to the other observations. The flickering in the light curve of this observation produces a broad peak around 0.014 Hz, corresponding to ~ 70 s oscillations in the light curve with an amplitude of a few hundred cnt s^{-1}.

The other observations do not show this kind of structure in the X-ray light curves. This type of flickering has also been seen in EXOSAT data by van der Klis & Jansen ([1985]), and in both cases they occurred in the phase intervals 0.0–0.75, which refers to ascending arm and top of the X-ray light curves (in our case $\phi \approx 0.52$ derived from the parabolic ephemeris given by Kitamoto et al. [1995]). Their suggestion for this phenomenon is that they could arise due to structures projecting above the surface of the disk, which are carried around by the rotation of the matter in the disk. During the observation that we observe this phenomenon, the source reached the highest intensity we saw it at around 6000 cnt$\,$s^{-1}. Hardness vs. time curves (HC) of this flickering segment do not confirm that the oscillations are correlated with the X-ray colours. Flickering has an effect on the power spectra that it adds extra power to it and makes VLFN component deviated a bit from power law (see Fig. 4).

There are a few models constructed for Cyg X-3 in which a scattering region around either the system ('cocoon' model), or the compact object ('accretion disk corona' model) or WR star ('wind scattering' model) (see Davidsen & Ostriker [1974]; Pringle [1974]; Milgrom & Pines [1978]; White & Holt [1982]; van Kerkwijk et al. [1996]) is proposed. van den Heuvel & de Loore ([1973]) also concluded that the system is surrounded by a thick cloud of gas as a result of the sharp low energy cut-off in the energy spectrum of Cyg X-3. According to these models, the X-rays must come from a circumstellar scattering region. This region reduces the amplitude of any fast X-ray variability by scattering of the emitted X-ray photons, which then arrive at different times to the observer. Possibly this is the reason that we cannot see any feature in the power spectra of Cyg X-3. The compact object might perhaps be seen partly and the structure of the compact object is more directly reflected when the flickerings appeareded in the X-ray light curves.

References

[1973] Becklin E., Neugebauer G., Hawkings F.J., et al., 1973, Nat 245, 302

[1994] Berger M., and van der Klis, M., 1994, A&A 292, 175

[1988] Bonnet-Bidaud J. M., and Chardin G., 1988, Physics Reports 170, 325

[1981] Bonnet-Bidaud J.M., and van der Klis M., 1981, A&A 101, 229

[1974] Davidsen A., and Ostriker J.P., 1974, ApJ 189, 331

[1995] Fender R.P., Burnell S.J.B., Garrington S.T., et al., 1995, MNRAS 274, 633

[1967] Giacconi R., Gorenstein P., Gursky H., and Waters J.R., 1967, ApJ 148, L119

[1997] Ghigo F.D., Waltman E.B., Pooley G.G., et al., 1997, BAAS 190, #45.04

[1972] Gregory P.C., Kronberg P.P., Seaquist E.R., et al., 1972, Nat 239, 440

[1992] Kitamoto S., Mizobuchi S., Yamashita K., and Nakamura H., 1992, ApJ 384, 263

[1995] Kitamoto S., Hirano, A., Kawashima, K., et al., 1995, PASJ 47, 233

[1983] Leahy D.A., Darbro W., Elsner R.F., et al., 1983, ApJ 266, 160

[1978] Milgrom M., and Pines D., 1978, ApJ 220, 272

[1974] Pringle J.M., Nat 247, 21

Table 2: Observational parameters of Poisson spectra and the fit results of the power spectra. Second half of the table gives the power law fit results of rms normalized power spectra. Three distinct lines belonging to each parameters correspond to energies of $2-97\,\mathrm{keV}$, $2-13\,\mathrm{keV}$, and $13-97\,\mathrm{keV}$, respectively

	obs. 1	obs. 2	obs. 3	obs. 4	obs. 5	obs. 6	obs. 7	obs. 8
$r_0\,(\mathrm{cntrate/PCU})$	403	465	510	487	455	550	...	...
	321	383	432	405	397	470	916	871
	82	83	78	82	77	79	79	82
$r_{\mathrm{VLE}}(\mathrm{cntrate/PCU})$	105	107	104	86	86	86	...	...
	105	110	105	86	85	86	98	92
	107	110	105	86	86	86	93	93
Sinc norm $(\times 10^{-3})$	1.9	2.2	2.4	1.9	1.8	2.1	...	...
	1.5	1.9	2.0	1.6	1.5	1.8	1.4	1.2
	0.4	0.4	0.4	0.3	0.3	0.3	0.3	0.3
P_1	1.9868	1.9847	1.9829	1.9839	1.9849	1.9820	...	...
	$\pm.0003$	$\pm.0002$	$\pm.0002$	$\pm.0004$	$\pm.0004$	$\pm.0004$		
	1.9898	1.9877	1.9859	1.9868	1.9870	1.9848	1.9806	1.9899
	$\pm.0003$	$\pm.0001$	$\pm.0001$	$\pm.0003$	$\pm.0003$	$\pm.0003$	$\pm.0005$	$\pm.0005$
	1.9977	1.9976	1.9976	1.9969	1.9977	1.9975	1.9978	1.9983
	$\pm.0003$	$\pm.0001$	$\pm.0001$	$\pm.0003$	$\pm.0003$	$\pm.0003$	$\pm.0001$	$\pm.0001$
$P_2\ (\times 10^{-3})$	$1.0\pm.4$	$0.8\pm.3$	$1.0\pm.3$	$1.5\pm.5$	$0.7\pm.6$	$1.4\pm.5$	...	...
	$0.6\pm.4$	$0.6\pm.4$	$0.7\pm.3$	$0.9\pm.2$	$0.5\pm.4$	$1.1\pm.4$	not available	not available
	$0.4\pm.4$	$0.5\pm.4$	$0.3\pm.3$	$0.6\pm.2$	$0.5\pm.4$	$0.4\pm.4$	$1.6\pm.1$	$0.7\pm.1$
Poisson level	1.9886	1.9869	1.9852	1.9857	1.9866	1.9840	...	...
	$\pm.0005$	$\pm.0004$	$\pm.0004$	$\pm.0006$	$\pm.0006$	$\pm.0006$		
	1.9913	1.9896	1.9880	1.9883	1.9885	1.9867	1.9820	1.9911
	$\pm.0005$	$\pm.0004$	$\pm.0003$	$\pm.0004$	$\pm.0005$	$\pm.0005$	$\pm.0005$	$\pm.0005$
	1.9981	1.9980	1.9979	1.9972	1.9980	1.9978	2.000	1.9987
	$\pm.0005$	$\pm.0004$	$\pm.0003$	$\pm.0004$	$\pm.0005$	$\pm.0005$	$\pm.0005$	$\pm.0005$
VLFN amplitude (%)	$2.9\pm.3$	$2.9\pm.3$	$1.8\pm.2$	$1.7\pm.6$	$3.5\pm.6$	$0.9\pm.2$	...	...
(0.001–1 Hz)	$3.3\pm.3$	$3.3\pm.3$	$1.8\pm.1$	$1.9\pm.8$	$3.5\pm.5$	$1.0\pm.2$	$3.7\pm.2$	$3.2\pm.5$
	$3.4\pm.2$	$2.6\pm.1$	$1.7\pm.1$	$2.2\pm.2$	5.3 ± 1.6	not available	$3.8\pm.2$	6.1 ± 1.6
Power law index	$1.58\pm.09$	$1.91\pm.11$	$1.60\pm.11$	$1.67\pm.35$	$1.73\pm.15$	$1.23\pm.43$	...	...
	$1.76\pm.08$	$2.01\pm.08$	$1.65\pm.08$	$1.89\pm.39$	$1.74\pm.12$	$1.33\pm.31$	$1.80\pm.05$	$2.27\pm.15$
	$1.17\pm.06$	$1.32\pm.11$	$1.08\pm.24$	2.02 ± 1.07	$2.38\pm.38$	not available	$1.54\pm.08$	$2.83\pm.40$
χ^2/dof	0.42	0.63	0.61	0.48	0.53	0.35	...	...
	0.93	1.22	1.22	1.05	0.82	0.73	1.48	0.55
	1.04	0.93	1.07	0.94	0.92	not available	2.21	1.06

[1995] Schalinski C.J., Johnston K.J., Witzel A., et al., 1995, ApJ 447, 752

[1996] Smit J.M., and van der Klis M., 1996, A&A 316, 115

[2002] Stark, M.J., and Saia, M., 2002, American Astronomical Society, 201st AAS Meeting ♯ 54.08, Bulletin of the American Astronomical Society, Vol.34, 1199

[2004] Szostek, A., Zdziarski, A.A., and Lachowicz, 2004, in 'X-ray Timing 2003: Rossie and Beyond', AIP Conference Proceedings 714, 113

[1973] van den Heuvel E.P.J., and de Loore C., 1973, A&A 25, 387

[1988] van der Klis M., 1988, Timing Neutron Stars. In: Ögelman H. and van den Heuvel E.P.J. (eds) NATO ASI Series C262, p. 27

[1993] van der Klis M., 1993, Space Sci. Rev. 62, 173

[1981] van der Klis M., and Bonnet-Bidaud J.M., 1981, A&A 95, L5

[1982] van der Klis M., and Bonnet-Bidaud J.M., 1982, A&AS 50, 129

[1985] van der Klis M., and Jansen F.A., 1985, Nat 313, 768

[1993] van Kerkwijk M.H., 1993, PhD thesis, Institute 'Anton Pannekoek', University of Amsterdam

[1996] van Kerkwijk M.H., Geballe T.R., King D.L., et al., 1996, A&A 314, 521

[1982] White N.E., and Holt S.S., 1982, ApJ 257, 318

[2003] Vilhu, O., Hjalmarsdotter, L., Zdziarski, A.A., et al., 2003, A&A 411, L405

[1995] Zhang W., 1995, RXTE/PCA Internal Memo, 5–23–95

[1995] Zhang W., Jahoda K., Swank J.H., et al., 1995, ApJ 449, 930